

# A Compact Tri-Band Flexible MIMO Antenna Based on Liquid Crystal Polymer for Wearable Applications

Chengzhu Du<sup>1, \*</sup>, Xun Wang<sup>1</sup>, Gaoya Jin<sup>1</sup>, and Shunshi Zhong<sup>2</sup>

**Abstract**—In this paper, a compact tri-band flexible MIMO antenna based on liquid crystal polymer (LCP) is designed to operate in WLAN and WiMAX bands. The antenna consists of two identical antenna elements. The isolation structure includes a ground slot, two I-shaped branches, and a parasitic strip. The measured results show that the impedance bandwidth ( $S_{11} < -10$  dB) covers three frequency bands of 2.38–2.55 GHz, 3.37–3.60 GHz, and 4.92–5.37 GHz, and the  $S_{21}$  of working bands is basically better than  $-19$  dB. Moreover, the flexibility of the MIMO antenna is analyzed at different bent cases. The specific absorption ratio (SAR) values are obtained by simulating the model of antenna approaching human body. The simulated results show that the SAR value of the antenna meets the European Union (EU) standard. The proposed antenna demonstrates the characteristics of satisfactory radiation, high isolation, sound gain in working bands and flexibility, which has good application prospects in the wearable field.

## 1. INTRODUCTION

In recent years, wireless technology and communication technology have entered a state of rapid development all over the world. The fifth generation of mobile communication technology (5G) which can greatly improve system capacity and energy efficiency has emerged and quickly attracted widespread attention from scholars. Multiple Input Multiple Output (MIMO) technology is also widely recognized as one of the most researched frontier technologies. In order to effectively expand the channel capacity of the system and improve the quality of communication, it is necessary to eliminate the multipath effect, and MIMO technology can effectively solve this problem by introducing multiple antennas at the transceiver.

If the correlation between the receiving end and transmitting end is too high, the performance of the MIMO antenna is deteriorated. Therefore, a sufficiently high isolation is a necessary condition for the MIMO antenna. With the wide application of MIMO technology on a global scale, such as neutralization-line technique [1,2], ground branches [3], parasitic elements [4], defected ground structure [5], and metamaterials [6], many improved isolation methods have been extensively studied.

As frequencies tend to increase for the next generation of wireless applications, the materials and integration techniques in RF systems are experiencing more demanding performance constraints. In this paper, liquid crystal polymer (LCP) [7–11] material is used as the dielectric substrate. Liquid crystal polymer (LCP) is a new flexible substrate material with excellent application prospects in microwave and millimeter wave circuits.

The low loss ( $\tan \delta = 0.002$  for  $f < 35$  GHz), near hermetic nature (water absorption 0.04%), and low cost makes it appealing for high-frequency designs where excellent performance is required for minimal cost. The low water absorption rate of LCP prevents the relative dielectric constant and loss tangent from changing, so that it remains stable in various environments. LCP is a good choice for

---

Received 20 April 2021, Accepted 19 May 2021, Scheduled 2 June 2021

\* Corresponding author: Chengzhu Du (duchengzhu@163.com).

<sup>1</sup> College of Electronics and Information Engineering, Shanghai University of Electric Power, Shanghai 200090, China. <sup>2</sup> School of Communication and Information Engineering, Shanghai University, Shanghai 200072, China.

high performance, small size device design. The LCP is a flexible material which has good flexibility and can be bent at will.

A number of flexible MIMO antennas have been reported in many literatures for the wireless applications [12–14]. References [12] and [13] proposed two wearable MIMO antennas for Industrial Scientific Medical (ISM) band. These two antennas perform well and demonstrate human body analysis. However, the material of the antenna substrate proposed in [12] is rigid FR4, and the port isolation is less than  $-15$  dB, while the antenna isolation in [13] is only less than  $-12$  dB. Neither of these two antennas can meet the high isolation requirements. A textile dual-band MIMO antenna based on a substrate integrated waveguide structure has been proposed in [14] with coaxial feed, and the port isolation is better than 20 dB. When being bent and working on human tissue, the antenna performance does not change much. The above three types of wearable antennas are single-frequency or dual-frequencies, which is far from meeting the current requirements for multi-frequency antennas.

This paper designs a compact tri-band MIMO antenna based on liquid crystal polymer (LCP), which can work in the 2.45/5.2 GHz bands of WLAN and the 3.5 GHz band of WiMAX [15–20]. The proposed MIMO antenna contains two symmetric antenna elements with two inverted-F branches. The isolation structure includes a ground slot, two I-shaped branches, and a parasitic strip. The measured results show that the flexible MIMO antenna has good isolation better than 19 dB. The size of the antenna is  $59\text{ mm} \times 29\text{ mm} \times 0.1\text{ mm}$ . Moreover, the  $S$ -parameter ( $S_{11}$  and  $S_{21}$ ) is simulated and measured after the antenna is bent. The performance of the antenna in different positions of the human body is measured, and the SAR value is simulated by using HFSS when the antenna is on the human body model [21, 22].

## 2. ANTENNA DESIGN AND ANALYSIS

### 2.1. Antenna Structure

The structure of the antenna is shown in Figure 1. The LCP substrate is Rogers ULTRALAM 3850 with a dielectric constant of 2.9, loss tangent of 0.002, and thickness of 0.1 mm. The feeding mode is microstrip feed, and the characteristic impedance is designed to be  $50\ \Omega$ .

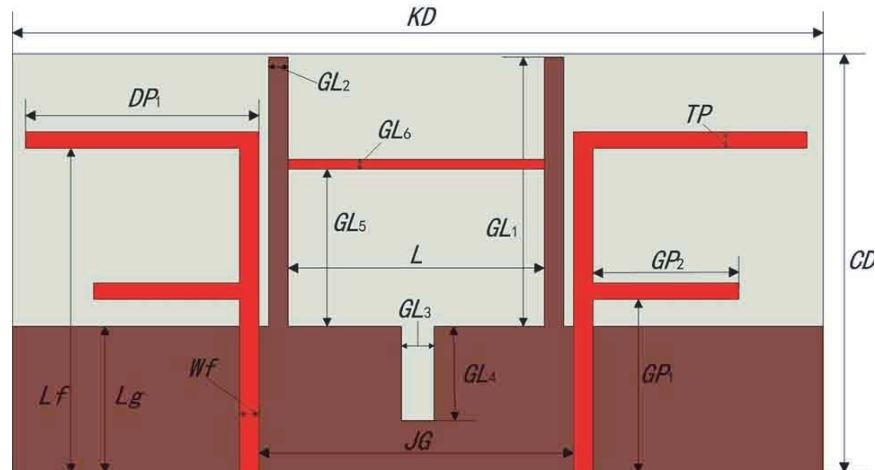


**Figure 1.** Structure of the antenna.

The parameters in Figure 1 are the structural dimensions of the antenna. The proposed MIMO antenna is optimized by HFSS software, and the optimal parameters are listed in Table 1.

### 2.2. Design Process

In order to better understand the design process of the antenna, three evolutionary iterations of the antenna are shown in Figure 2. Initially, the MIMO antenna element is an inverted-F branch, as shown

Table 1. Antenna geometry.

| parameters | element/mm | parameters | element/mm |
|------------|------------|------------|------------|
| $KD$       | 59         | $Lg$       | 9          |
| $CD$       | 29         | $GL_1$     | 17.4       |
| $Wf$       | 0.5        | $GL_2$     | 0.8        |
| $Lf$       | 25.4       | $GL_3$     | 2          |
| $GP_1$     | 12.5       | $GL_4$     | 5.4        |
| $GP_2$     | 9.1        | $GL_5$     | 18.4       |
| $DP_1$     | 18.2       | $GL_6$     | 0.2        |
| $TP$       | 0.4        | $L$        | 18.5       |
| $JG$       | 21.1       |            |            |

in Antenna I of Figure 2. The long branch resonates in the low frequency band of the WLAN –2.45 GHz; the short branch resonates in the high frequency band of the WLAN –5.2 GHz; and the lengths are 21.6 mm and 18.2 mm, respectively. It can be observed from Figure 3 that the  $S_{11}$  of Antenna I is lower than –10 dB over 2.3–2.42 GHz and 5.17–5.43 GHz while mutual coupling is serious over the 5.2 GHz bands.

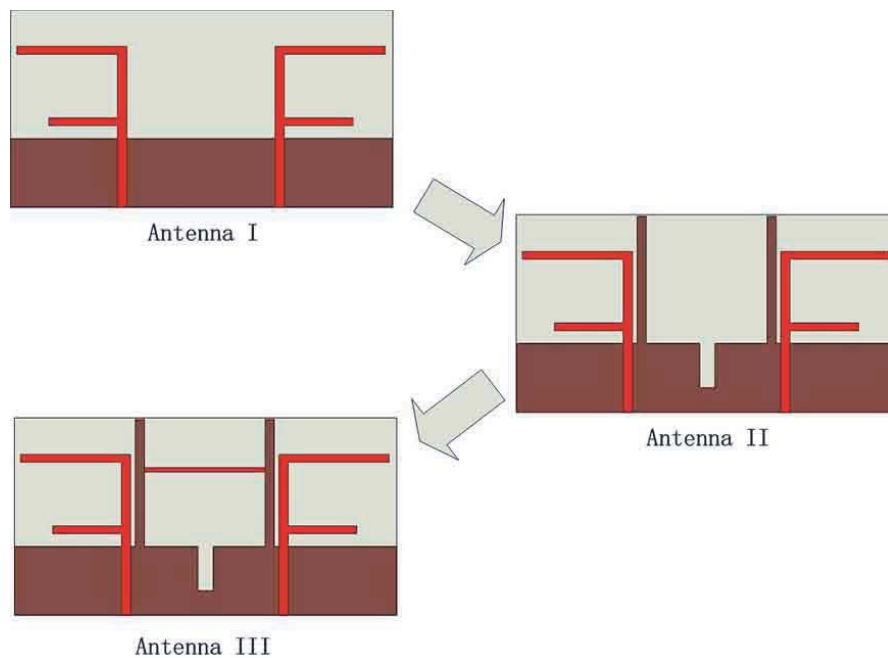
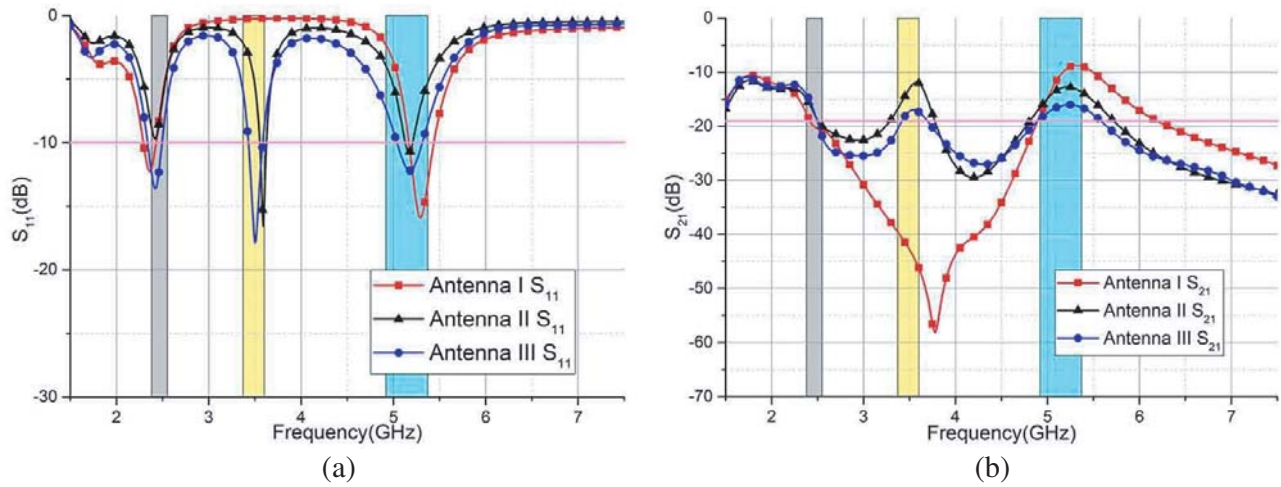


Figure 2. Antenna design process.

Secondly, in Antenna II, two I-shaped branches and a slot are added at the back side of the antenna as the isolation structure. It can be seen from Figure 3 that Antenna II resonates at three different frequencies, and the impedance bandwidth less than –10 dB covers 3.56–3.62 GHz and 5.13–5.2 GHz, while  $S_{21}$  is less than –12 dB at 2.38–2.55 GHz, 3.37–3.60 GHz, and 4.92–5.37 GHz. Since the thickness of the flexible material LCP is very thin, and the two branches are close to each other, the I-shaped branch and inverted-F branch are coupled to generate the third operating frequency of the antenna, the WiMAX –3.5 GHz. Thus, the I-shaped branch of the antenna has two functions of improving isolation and generating operating frequency simultaneously.



**Figure 3.** The comparison of the simulated  $S$  parameters of three evolutionary antennas. (a)  $S_{11}$ . (b)  $S_{21}$ .

Thirdly, in Antenna III, a parasitic strip is placed between the two antenna elements. It can be seen from Figure 3 that the  $S_{11}$  of Antenna III is lower than  $-10$  dB over 2.34–2.49 GHz, 3.43–3.58 GHz, and 5.04–5.31 GHz, while the  $S_{21}$  of Antenna III is better than  $-18$  dB at all working bands. The isolation is enhanced by inserting a parasitic strip which can cancel out original coupling. The parasitic strip is not directly connected to the antenna element and perpendicular to the microstrip, which has less influence on the antenna matching characteristics.

### 2.3. Parametric Study

Simulated results of  $S_{11}$  with different values of  $GL_1$  are shown in Figure 4. In this antenna, two I-shaped ground branches and two F-type antenna elements are coupled to generate the third operating frequency of the WiMAX band.  $GL_1$  is the length of the I-shaped branch.

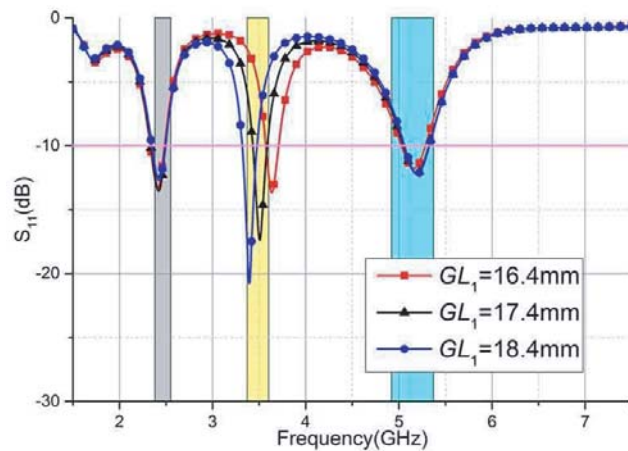


**Figure 4.** Simulated results of  $S_{11}$  with different values of  $GL_1$ .

With the increase of  $GL_1$ , the 3.5 GHz band of the antenna continuously shifts to the low-frequency part. It can be clearly seen that the length of the I-shaped branch only affects the 3.5 GHz band.

## 2.4. Fabricated Antenna

Finally, based on the optimized antenna parameters in Table 1, the fabricated antenna is processed. The concrete results are shown in Figure 5.



**Figure 5.** Fabricated antenna. (a) Front. (b) Back.

## 3. RESULTS AND DISCUSSIONS

Based on ANSOFT HFSS 13 and Agilent Technologies N5230A PNA-L network analyzer, the performance of various aspects of the flexible MIMO antenna is discussed by the measured and simulated results of the antenna.

### 3.1. The Current between Isolation Structure and the E-Field Distribution

The surface current distribution of MIMO antennas at 2.45 GHz, 3.5 GHz, and 5.2 GHz is shown in Figure 6, when port 1 is excited and port 2 connected with  $50\ \Omega$  load. The effect of the isolation structure can be observed by the current distribution. It can be seen that when the two I-shaped branches are added on the back side of the antenna, the flow path of the distributed current on the surface of the antenna ground can be changed, thereby improving the impedance matching characteristics of the element antenna. In addition, the ground branch can act as a reflector, and the isolation can be effectively performed for two antenna elements.

The ground slot is placed in the middle of the two I-shaped ground branches, which can weaken the ground surface current flowing from the excitation port to the non-excited port. The isolation is enhanced by inserting a parasitic strip between the two antenna elements, which can cancel out original coupling.

In order to analyze the working performance and radiation characteristics, the current distributions of the antenna are simulated while port 1 is excited and port 2 connected with  $50\ \Omega$  load. Figure 7(a) shows the current on the long branches at 2.45 GHz. Figure 7(b) shows that the current is focused on the branches at 3.5 GHz, which means that the antenna can effectively receive the WiMAX band. Figure 7(c) shows the current at short branches at 5.2 GHz. The E-field distribution can be seen in Figure 7(d), which shows that E-field radiates from port 1 to port 2, indicating that the antenna has better performance.

### 3.2. S-Parameter

Simulated and measured  $S_{11}$  of the MIMO antenna are shown in Figure 8. The  $S_{11}$  of the antenna is less than  $-10\ \text{dB}$  in the three frequency ranges of 2.34–2.50 GHz, 3.43–3.59 GHz, and 5.03–5.32 GHz, which satisfies the operating requirements of the WLAN band and WiMAX band. The measured results

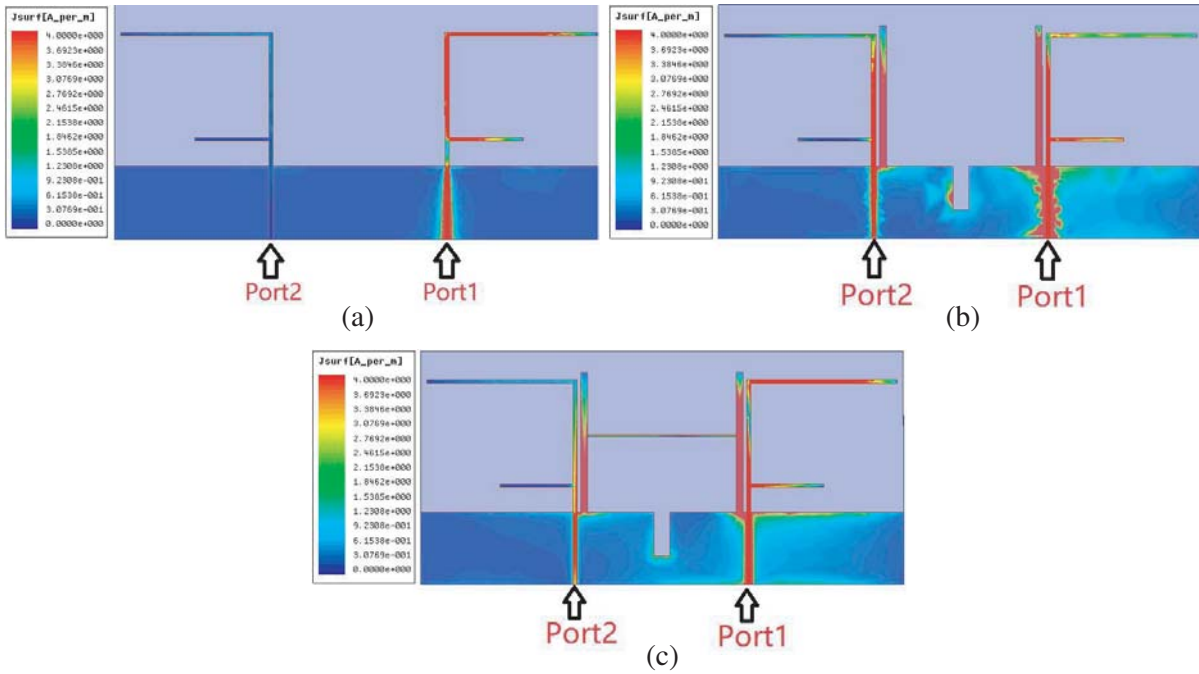


**Figure 6.** Surface current distribution of MIMO antennas at 3.5 GHz when port 1 is excited and port 2 is connected with  $50\ \Omega$  load. (a) Antenna I. (b) Antenna II. (c) Antenna III.

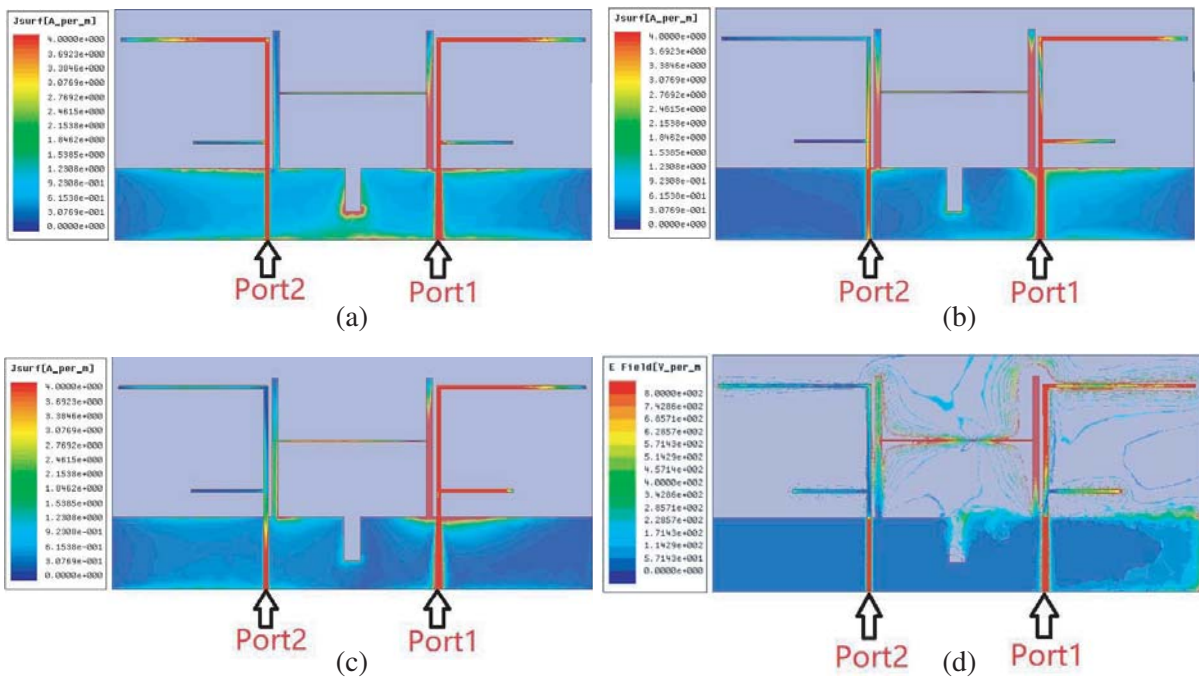


**Figure 7.** Surface current distribution of MIMO antennas when port 1 is excited and port 2 is connected with  $50\ \Omega$  load. (a) 2.45 GHz. (b) 3.5 GHz. (c) 5 GHz. (d) E-field distribution at 3.5 GHz.

of the antenna  $S_{11}$  show that it operates at 2.38–2.55 GHz in the low-frequency band. Compared with the  $S_{11}$  simulated results, due to the inaccurate in physical processing and the external interference in the measurement environment, some shifts occur in the low-frequency part, but still can meet the

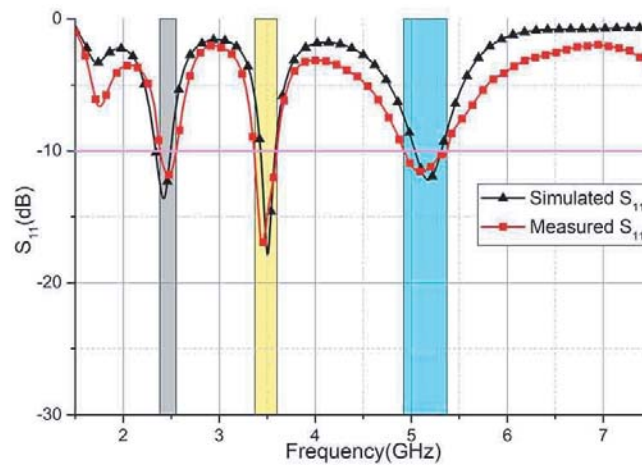


**Figure 8.** Simulated and measured  $S_{11}$ .

requirements of the WLAN band. In the middle-frequency part, the antenna operates at 3.37–3.60 GHz, which is basically the same as the simulated  $S_{11}$  result. In the high-frequency band, the antenna operates at 4.92–5.37 GHz, which is slightly wider than the simulated bandwidth.

Simulated and measured  $S_{21}$  of the MIMO antenna are shown in Figure 9. It can be seen from the figure that there is a certain difference between the simulated and measured values of  $S_{21}$ . In general, the measured  $S_{21}$  of the antenna is less than  $-19$  dB.

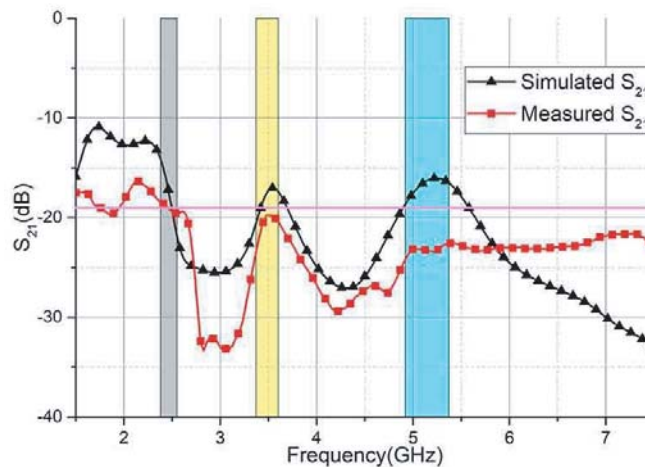


**Figure 9.** Simulated and measured  $S_{21}$ .

The flexible antenna is mainly oriented to the research in the wearable wireless communication system, and the antenna is inevitably bent in the actual application. LCP is a flexible material, which has good flexibility and can be bent at will. Therefore, the  $S_{11}$  and  $S_{21}$  values of the antenna are analyzed after the antenna is bent.

Simulated  $S_{11}$  of the antenna when the antenna is unbent and bent is shown in Figure 10. The antenna is bent along the  $E$ -plane and  $H$ -plane, respectively. As shown in Figure 10(a), the antenna is bent along the  $E$ -plane at different radii. It can be clearly seen that when the radius becomes larger, the simulated effect of the antenna will be better. Compared with the unbent state, the bandwidths of the bent antenna at 2.45/3.5/5.2 GHz band deteriorate to some extent. As shown in Figure 10(b), the antenna is bent along the  $H$ -plane at different radii. The simulated bandwidths of the 2.45 GHz

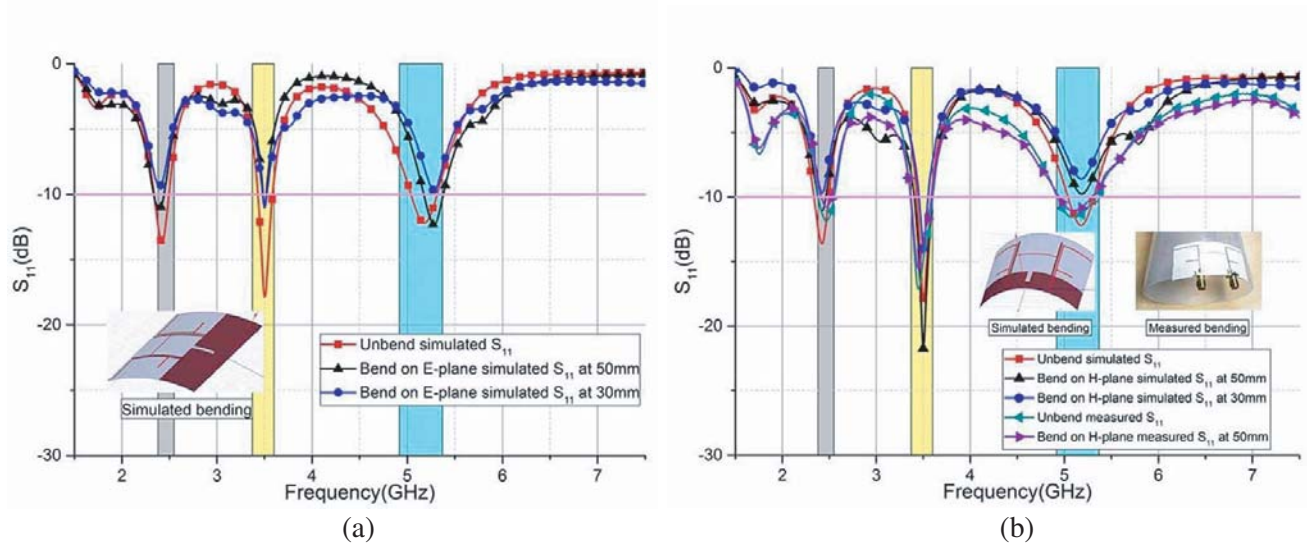


**Figure 10.** Simulated and measured  $S_{11}$  of the antenna when the antenna is unbent and bent. (a)  $E$ -plane bending. (b)  $H$ -plane bending.

band and 5.2 GHz band have deteriorated to some extent, and the bandwidth of the 3.5 GHz band is basically unchanged. The measured  $S_{11}$  of the antenna when the antenna is unbent and  $H$ -plane bent are shown in Figure 10(b), and the bandwidth of the antenna is changed slightly.

The simulated and measured  $S_{21}$  of the antenna when the antenna is unbent and bent are shown in Figure 11. No matter whether the antenna is bent along the  $E$ -plane or the  $H$ -plane, there is no negative impact on the isolation of the antenna, and the flexible MIMO antenna still has good isolation.

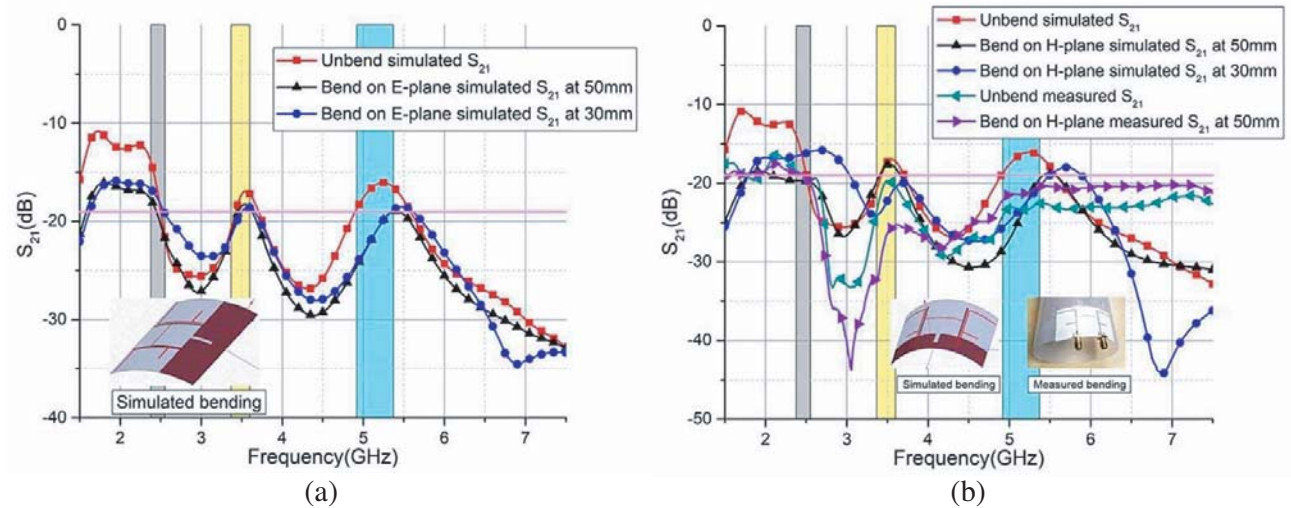


**Figure 11.** Simulated and measured  $S_{21}$  of the antenna when the antenna is unbent and bent. (a)  $E$ -plane bending. (b)  $H$ -plane bending.

### 3.3. Radiation Pattern

The simulated and measured results of radiation patterns are shown in Figure 12. It shows the patterns of the three frequency points of 2.45 GHz, 3.5 GHz, and 5 GHz, including the  $E$ -plane and  $H$ -plane. It can be seen that the patterns are quasi-omnidirectional, which is suitable for wireless communication terminals to receive signals from any direction.

### 3.4. Diversity Performance of the Antenna

The envelope correlation coefficient (ECC) is one of the important parameters which can be used to measure the diversity gain of a MIMO system [23]. In general, the high diversity gain can be obtained

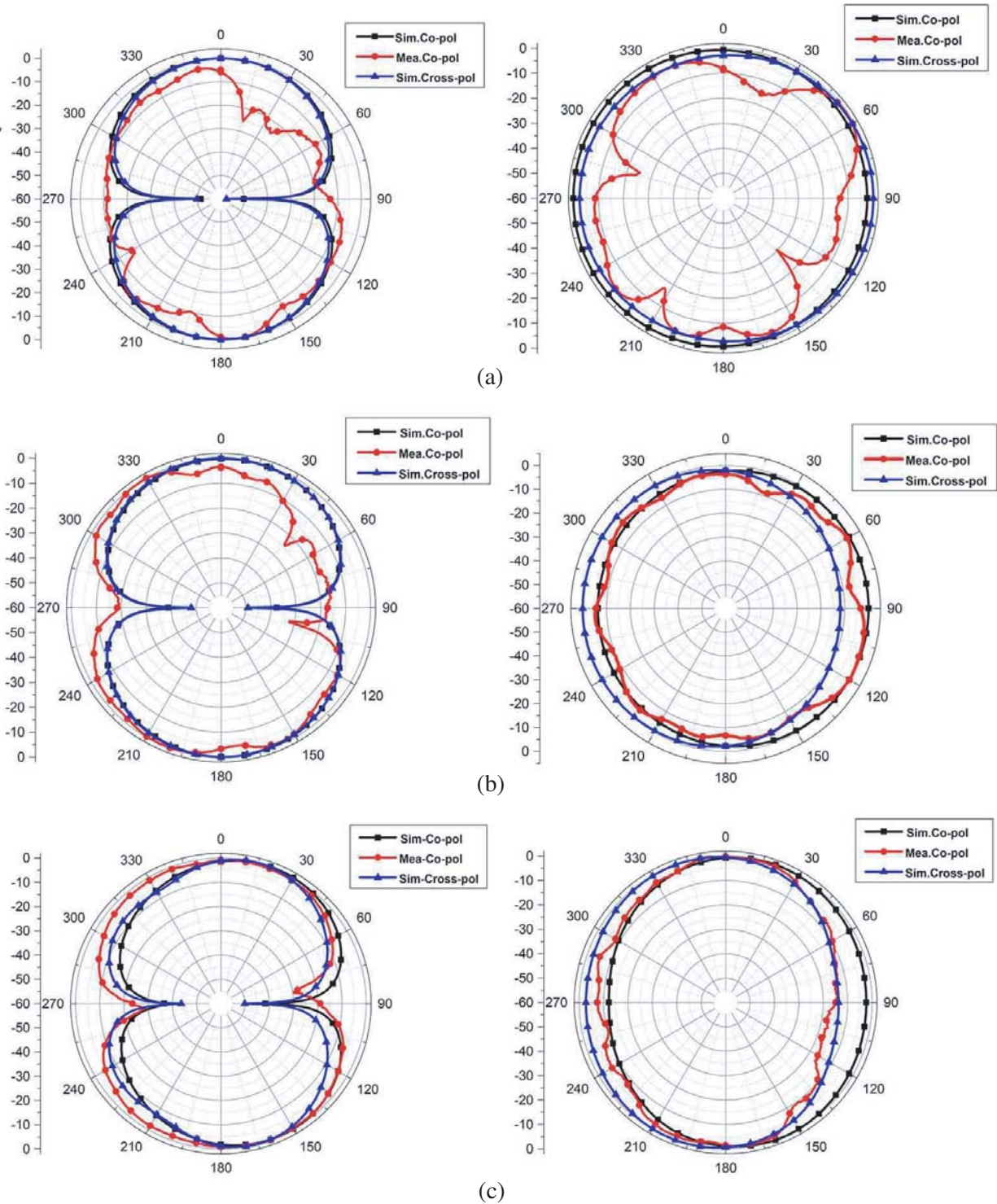


**Figure 12.** Simulated and measured results of radiation patterns. (a) 2.45 GHz. (b) 3.5 GHz. (c) 5 GHz.

from low envelope correlation. ECC for a two antenna system can be calculated using the simple formula [24]:

$$ECC = \left| \frac{S_{11}^* S_{12} + S_{21}^* S_{22}}{\left(\sqrt{1 - |S_{11}|^2 - |S_{21}|^2}\right) \cdot \left(\sqrt{1 - |S_{22}|^2 - |S_{12}|^2}\right)} \right| \quad (1)$$

According to the simulated and measured  $S$ -parameters, the ECC of the antenna is calculated. Due to the symmetry of the port,  $S_{22}$  is approximately equal to  $S_{11}$ , and  $S_{12}$  is approximately equal to  $S_{21}$ . Substituting the  $S$ -parameter value into the above formula, ECC is shown in Figure 13(a). In the three operating bands of 2.38–2.55 GHz, 3.37–3.60 GHz, and 4.92–5.37 GHz, the ECC simulated curves are all less than 0.1, and the ECC measured curves are all less than 0.05, which is much smaller than the general requirements of the MIMO antenna for the correlation coefficient.

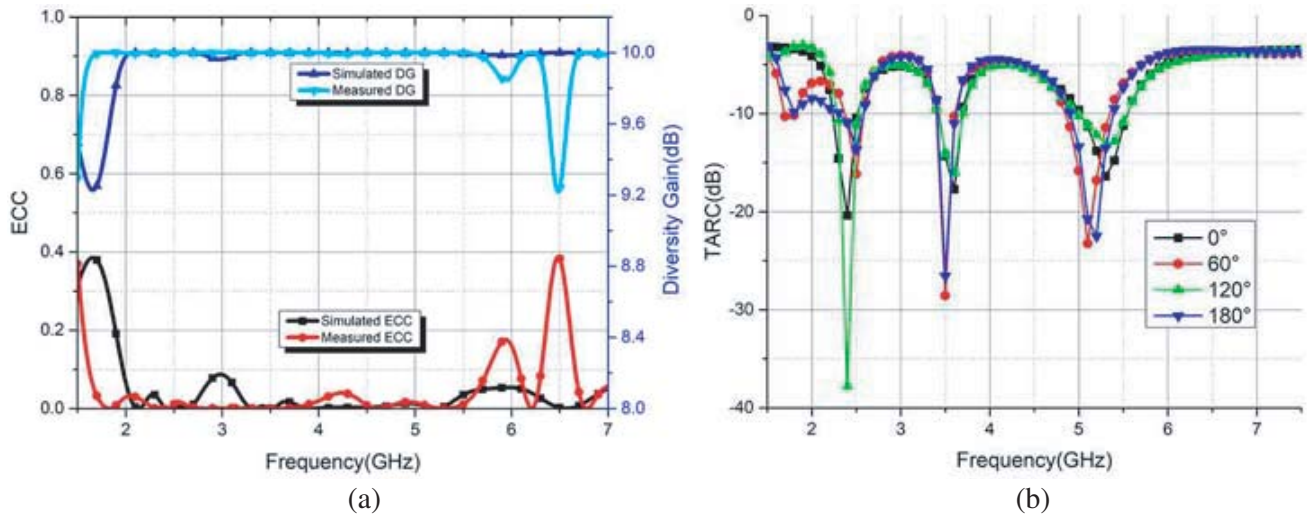


**Figure 13.** Simulated or measured results of the proposed antenna. (a) ECC and DG. (b) TARC.

Similarly, diversity gain (DG) is another characteristic to evaluate the correlation between MIMO antenna elements. The value of DG can be calculated as:

$$DG = 10\sqrt{1 - ECC^2} \quad (2)$$

As shown in Figure 13(a), the DG curves of all operating frequency bands are higher than 9.95.

Obviously, the TARC is the total active reflection coefficient that considers the isolation between antenna units, which can be expressed as:

$$TARC = \sqrt{\frac{(S_{11} + S_{12}e^{j\theta})^2 + (S_{21} + S_{22}e^{j\theta})^2}{2}} \quad (3)$$

It can be seen from Figure 13(b) that the TARC curve is similar to the  $S_{11}$  curve, which shows that the MIMO antenna has great diversity performance.

### 3.5. On-Body Effects on the MIMO Antenna

The antenna is based on flexible materials and has good application prospects in the wearable field. Wearable antennas must conform to the high immunity of the human-body loading. Therefore, we investigate the on-body antenna characteristics by placing the antenna on the wrist and chest. The MIMO antenna on the wrist and chest is shown in Figure 14.

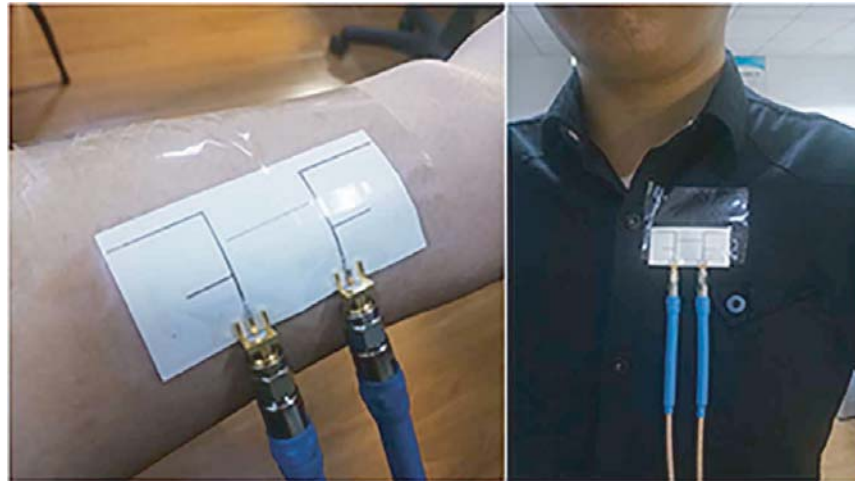


**Figure 14.** MIMO antenna on the wrist and chest.

Measured  $S$ -parameters on wrist, chest, and off-body are shown in Figure 15. It can be clearly seen that when the antenna is on wrist and chest, the  $S_{11}$  are deteriorated. When the antenna is on the wrist,  $S_{11}$  of the three operating bandwidths are slightly decreased, but still meet the requirements of MIMO antennas. When the antenna is on the chest,  $S_{11}$  experiences more serious deterioration, and the measured effect of the wrist is better than that of the chest.

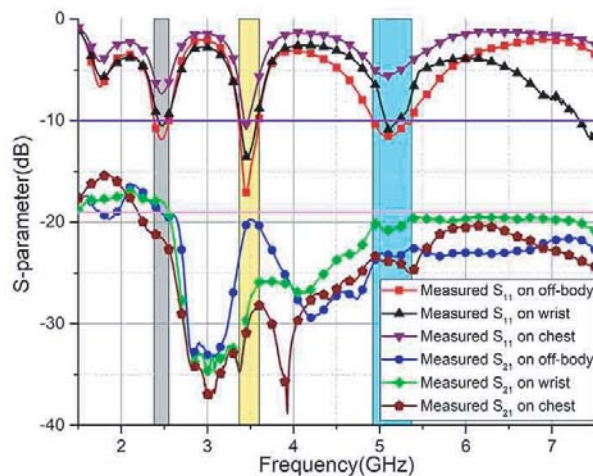


**Figure 15.** Measured  $S$ -parameter on wrist, chest and off-body.

Compared with the off-body, the  $S_{21}$  has a large floating. In general, the  $S_{21}$  still meets the requirements of the MIMO antenna when it is on wrist and chest, and has good isolation performance.

Specific Absorption Ratio (SAR) [25] is usually used to quantitatively measure the influence of antenna radiation energy on human tissues in the application of wearable antennas. The calculation formula of local SAR is as follows:

$$SAR = \sigma E^2 / \rho \tag{4}$$

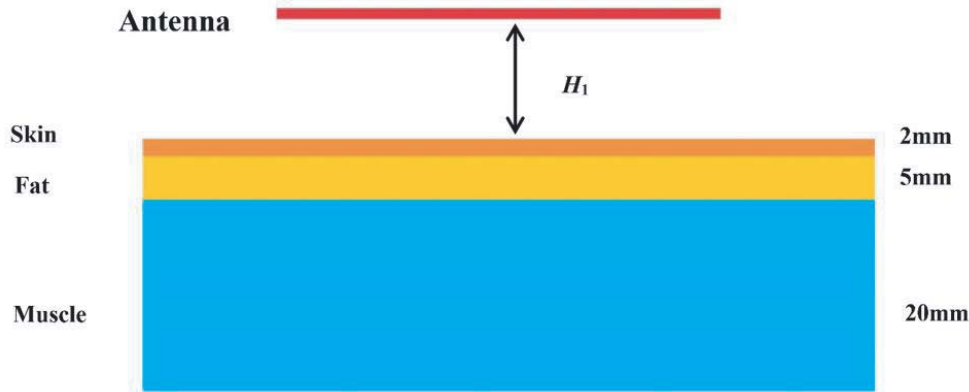
$\sigma$  is the electrical conductivity;  $E$  is the root mean square value of electric field intensity;  $\rho$  is the human tissue density.

As shown in Figure 16, the human tissue model consists of a 2 mm skin layer, a 5 mm fat layer, and a 20 mm muscle layer, and the input power is 0.1 w. The parameters of each layer of material are

**Table 2.** Material properties of the human tissue.

|                              | Skin  | Fat  | Muscle |
|------------------------------|-------|------|--------|
| $\epsilon_r$                 | 37.95 | 5.27 | 52.67  |
| $\sigma$ (S/m)               | 1.45  | 0.11 | 1.77   |
| Density (kg/m <sup>3</sup> ) | 1001  | 900  | 1006   |
| Thickness (mm)               | 2     | 5    | 20     |

listed in Table 2. The size of the whole human tissue model is 70 mm × 39 mm × 27 mm. According to the electromagnetic parameters of the three-layer human tissue model (including skin, fat, and muscle), the proximity of layered human body tissue model was built under the HFSS.

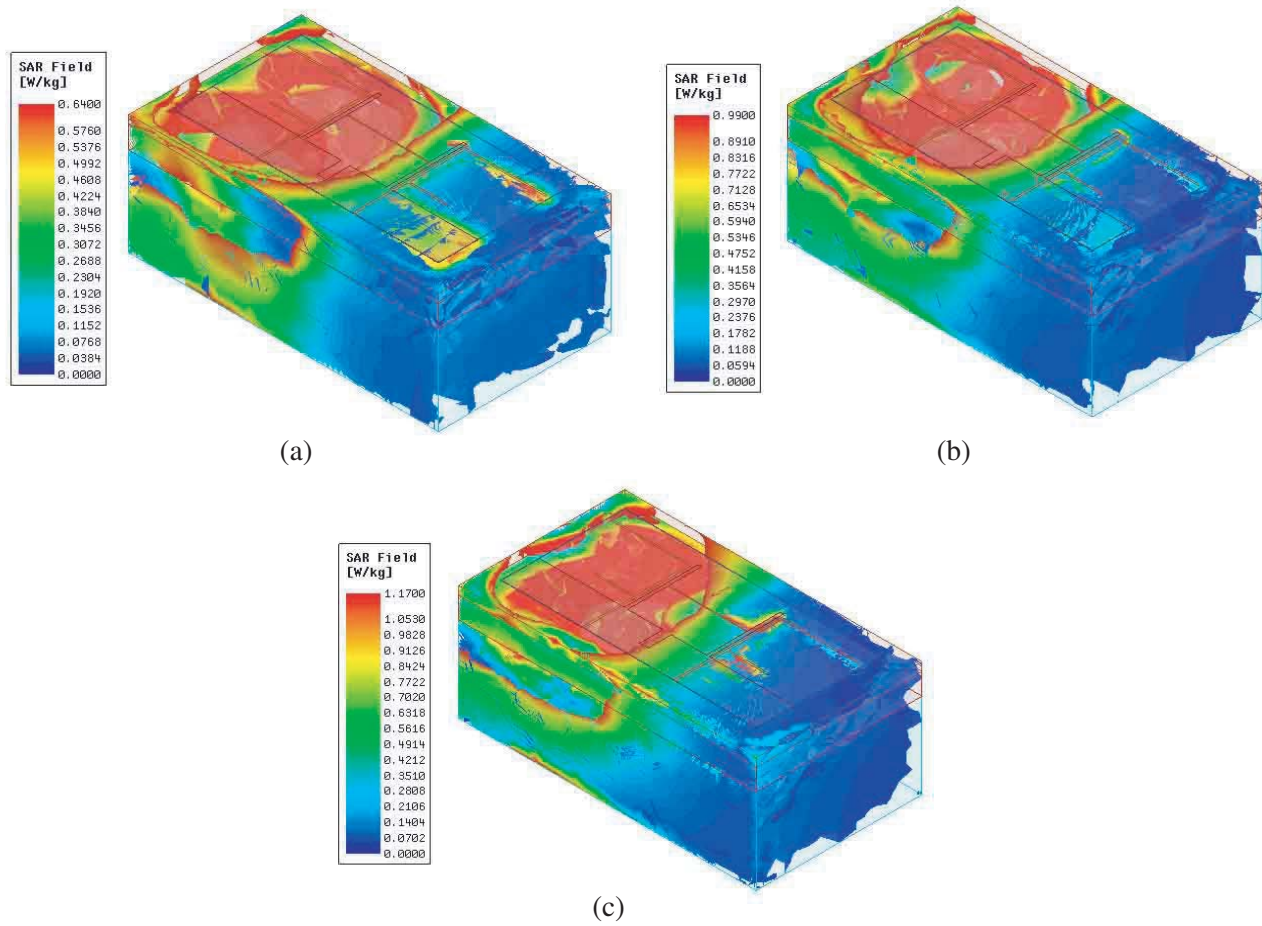
**Figure 16.** The human body approaching the antenna model.

The distance between the antenna and the human body surface is taken as variable  $H_1$  ( $H_1 = 0, 1, 2, 4$  and  $6$  mm). When the input power is  $0.1$  W, and the center frequency are  $2.45$  GHz,  $3.5$  GHz, and  $5$  GHz, respectively, the maximum SAR values are shown in Table 3. When  $H_1 = 1$  mm, the results show that the maximum simulated SAR values are lower than the EU standard of  $2$  W/kg/10 g tissue. Figure 17 exhibits the SAR distribution when  $H_1$  is  $1$  mm.

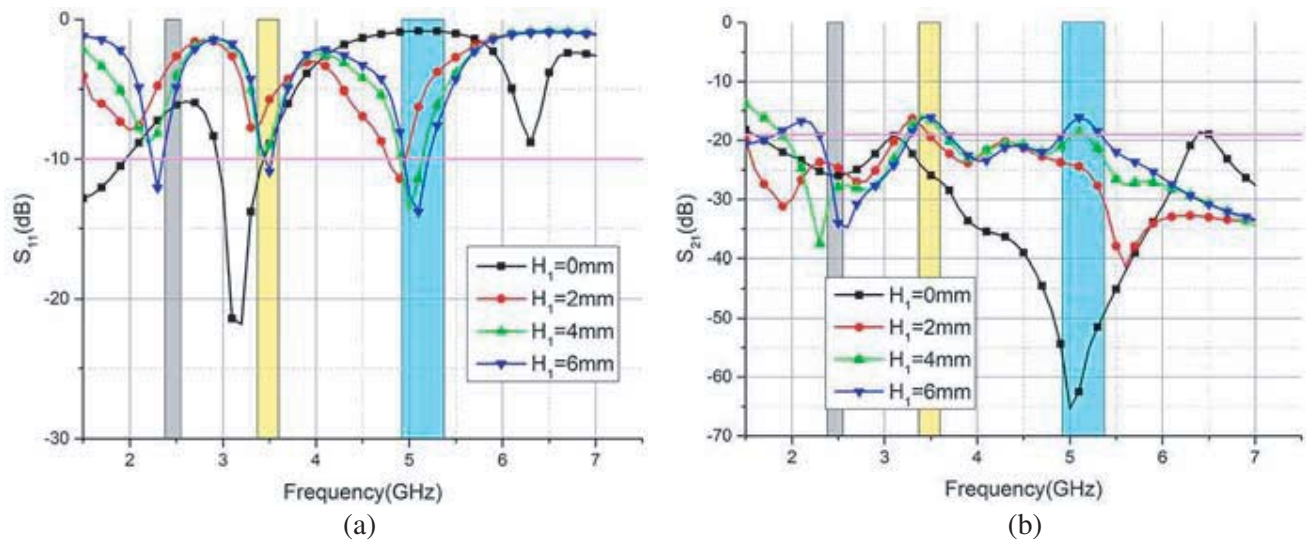
**Table 3.** Maximum SAR values with different frequencies.

| Frequency                          | 2.45 GHz | 3.5 GHz | 5 GHz |
|------------------------------------|----------|---------|-------|
| 10 g Tissue (W/kg) ( $H_1 = 0$ mm) | 1.79     | 2.09    | 0.67  |
| 10 g Tissue (W/kg) ( $H_1 = 1$ mm) | 0.64     | 0.99    | 1.17  |
| 10 g Tissue (W/kg) ( $H_1 = 2$ mm) | 0.76     | 0.87    | 1.34  |
| 10 g Tissue (W/kg) ( $H_1 = 4$ mm) | 0.95     | 0.77    | 1.17  |
| 10 g Tissue (W/kg) ( $H_1 = 6$ mm) | 1.00     | 0.74    | 0.97  |

Figure 18 shows the simulation results of  $S_{11}$  and  $S_{21}$  with the distances of  $0$  mm,  $2$  mm,  $4$  mm, and  $6$  mm at  $3.5$  GHz in the model of the antenna approaching the human body. When  $H_1$  goes down, the three resonant frequency points still exist, but they are offset to high frequency. When  $H_1 = 6$  mm, the antenna can still work with  $S_{11}$  less than  $-6$  dB at  $2.45$  GHz,  $3.5$  GHz, and  $5$  GHz bands. As shown in Figure 18(b), when  $H_1 = 0$  mm,  $2$  mm,  $4$  mm, and  $6$  mm, the  $S_{21}$  of the antenna all meet the requirements.



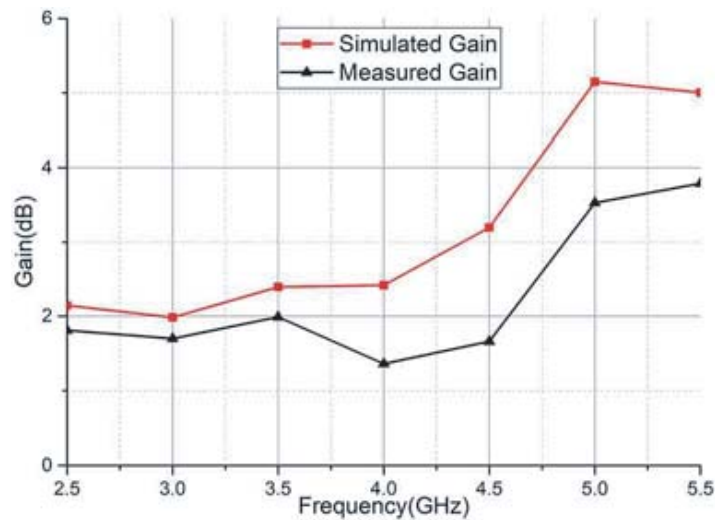
**Figure 17.** Simulated SAR distribution in 10g tissues on the human tissue model. (a) 2.45 GHz, (b) 3.5 GHz, and (c) 5 GHz.



**Figure 18.** Simulated at 3.5 GHz when  $H_1 = 0$  mm, 2 mm, 4 mm and 6 mm. (a)  $S_{11}$ . (b)  $S_{21}$ .

**Table 4.** Comparison between the proposed antenna with other reported multi-frequency antennas.

| Ref.  | Sub.       | Sub. type   | Size (mm <sup>2</sup> ) | Op. Frqn. (GHz)                     | Isolation. (dB) | ECC  | DG   | SAR (W/kg) |
|-------|------------|-------------|-------------------------|-------------------------------------|-----------------|------|------|------------|
| [12]  | FR4        | Rigid       | $\pi \times (21.1)^2$   | 2.4–2.49                            | > 15            | NA   | NA   | NA         |
| [13]  | Felt       | Flexibility | 38.1 × 38.1             | 2.3–2.8                             | > 12            | NA   | NA   | NA         |
| [14]  | Felt       | Flexibility | 92.3 × 101.6            | 2.36–2.53<br>5.14–5.86              | > 20            | 0.08 | 9.92 | NA         |
| [17]  | FB4-2      | Rigid       | 30 × 30                 | 3.28–3.41<br>4.03–4.12<br>4.72–4.86 | > 15            | 0.06 | 9.94 | NA         |
| [18]  | FR4        | Rigid       | 64 × 30                 | 2.7–3.0<br>4.2–4.6<br>6.9–8.2       | > 15            | 0.03 | 9.97 | NA         |
| [19]  | FB4-2      | Rigid       | 60 × 40                 | 3.46–3.48<br>3.97–4.19<br>4.61–4.85 | > 18            | 0.05 | 9.95 | NA         |
| [20]  | FR4        | Rigid       | 40 × 40                 | 2.31–2.25<br>3.1–4.13<br>5.32–5.71  | > 13            | NA   | NA   | NA         |
| [21]  | Felt       | Flexibility | 56 × 47                 | 2.3–2.5                             | > 20            | 0.07 | 9.9  | NA         |
| [22]  | Roger 3003 | Flexibility | 59.71 × 57.77           | 2.38–2.47<br>5.11–5.31              | NA              | NA   | NA   | 0.00037    |
| Prop. | LCP        | Flexibility | 59 × 29                 | 2.38–2.55<br>3.37–3.60<br>4.92–5.37 | > 19            | 0.05 | 9.95 | 0.64       |

**Figure 19.** Simulated and measured gain.

### 3.6. Gain

The simulated and measured gains of the MIMO antenna are shown in Figure 19. As can be seen from the figure, due to the inaccuracy in physical processing and the external interference in the measurement environment, the measured result of the antenna gain is slightly weaker than the simulated result. In addition, it can be clearly seen that the gains of the antenna in the three operating bands (2.5 GHz, 3.5 GHz, and 5 GHz) are higher than other bands. Because the antenna has better isolation at 5 GHz than at 3.5 GHz, and the simulated gain at 5 GHz is 3 dB higher than at 3.5 GHz. The measured maximum gain is 3.79 dB.

### 3.7. Performance Comparison

A comparison with a number of related recent research works is summarized in Table 4 which shows the performances of rigid and flexible MIMO antennas for wearable application. It can be clearly seen that the proposed flexible triple-band MIMO antenna has good performance.

## 4. CONCLUSION

In this paper, a compact tri-band flexible MIMO antenna based on LCP is designed to operate in two WLAN bands and WiMAX bands. The measured results show that the antenna operates in the three frequency bands of 2.38–2.55 GHz, 3.37–3.60 GHz, and 4.92–5.37 GHz. By adding I-shaped branches and a parasitic strip between antenna elements, high isolation of better than 19 dB and low envelope correlation coefficient of less than 0.05 can be obtained through the whole operating bands. In addition, the effect of the human body on the antenna performance is studied with the three-layer human tissue. When  $H = 1$  m, the maximum value of SAR meets the requirements of EU standards, and the values of  $S_{11}$  and  $S_{21}$  are also within the design range. The antenna has good application prospects in the wearable field.

## ACKNOWLEDGMENT

This work was supported by the National Natural Science Foundation of China under Grant No. 61371022.

## REFERENCES

1. Ling, X. and R. Li, "A novel dual-band MIMO antenna array with low mutual coupling for portable wireless devices," *IEEE Antennas and Wireless Propagation Letters*, Vol. 10, 1039–1042, 2011.
2. Su, S., C.-T. Lee, and F.-S. Chang, "Printed MIMO-antenna system using neutralization-line technique for wireless USB-Dongle applications," *IEEE Transactions on Antennas and Propagation*, Vol. 60, No. 2, 456–463, Feb. 2012.
3. Ding, Y., Z. Du, K. Gong, and Z. Feng, "A novel dual-band printed diversity antenna for mobile terminals," *IEEE Transactions on Antennas and Propagation*, Vol. 55, No. 7, 2088–2096, Jul. 2007.
4. Mak, A. C. K., C. R. Rowell, and R. D. Murch, "Isolation enhancement between two closely packed antennas," *IEEE Transactions on Antennas and Propagation*, Vol. 56, No. 11, 3411–3419, Nov. 2008.
5. Chiu, C.-Y., C.-H. Cheng, R. D. Murch, and C. R. Rowell, "Reduction of mutual coupling between closely-packed antenna elements," *IEEE Transactions on Antennas and Propagation*, Vol. 55, No. 6, 1732–1738, Jun. 2007.
6. Abdalla, M. A. and A. Ibrahim, "Compact and closely spaced metamaterial MIMO antenna with high isolation for wireless applications," *IEEE Antennas and Wireless Propagation Letters*, Vol. 12, 1452–1455, 2013.
7. Thompson, D. C. and J. H. Tantoto, "Characterization of Liquid Crystal Polymer (LCP) material and transmission lines on LCP substrates from 30–110 GHz," *IEEE Transactions on Microwave Theory and Techniques*, Vol. 52, 1343–1352, 2004.

8. Thompson, D., O. Tantot, J. Hubert, et al., "Characterization of LCP material and transmission lines on the LCP from 30 to 110 GHz," *IEEE Transactions on Microwave Theory and Techniques*, Vol. 52, No. 4, 1343–1352, 2004
9. Dejean, G., R. Bairavasubramanian, D. Thompson, et al., "Liquid Crystal Polymer (LCP): A new organic material for the development of multilayer dual-frequency/dual-polarization flexible antenna arrays," *IEEE Antennas and Wireless Propagation Letters*, Vol. 4, No. 1, 22–26, 2005
10. Kingsley, N., G. E. Ponchak, J. Papapolymerou, et al., "Recon Figureurable RF MEMS phased array antenna integrated within a Liquid Crystal Polymer (LCP) system-on-package," *IEEE Transactions on Antennas and Propagation*, Vol. 56, No. 1, 108–118, 2008
11. Wang, G., R. Bairavasubramanian, B. Pan, et al., "Radio-frequency MEMS-enabled polarization-recon Figureurable antenna arrays on multilayer liquid crystal polymer," *IET Microwaves Antennas and Propagation*, Vol. 5, No. 13, 1594–1599, 2011
12. Wen, D., Y. Hao, M. O. Munoz, H. Wang, and H. Zhou, "A compact and low-profile MIMO antenna using a miniature circular high impedance surface for wearable applications," *IEEE Transactions on Antennas and Propagation*, Vol. 66, No. 1, 96–104, 2018.
13. Li, H., S. Sun, B. Wang, and F. Wu, "Design of compact single-layer textile MIMO antenna for wearable applications," *IEEE Transactions on Antennas and Propagation*, Vol. 66, No. 6, 3136–3141, 2018.
14. Yan, S., P. J. Soh, and G. A. E. Vandenbosch, "Dual-band textile MIMO antenna based on Substrate-Integrated Waveguide (SIW) technology," *IEEE Transactions on Antennas and Propagation*, Vol. 63, No. 11, 4640–4647, 2015.
15. Huang, S. S., J. Li, and J. Z. Zhao, "A novel compact planar triple-band monopole antenna for WLAN/WiMAX applications," *Progress In Electromagnetics Research Letters*, Vol. 50, No. 1, 117–123, 2014.
16. Wang, Y. D., J. H. Lu, and H. M. Hsiao, "Novel design of semi-circular slot antenna with triple-band operation for WLAN/WiMAX communication," *Microwave and Optical Technology Letters*, Vol. 50, No. 6, 1531–1534, 2008.
17. Niu, B. and J. Tan "Compact tri-band MIMO antenna based on quarter-mode slotted substrate-integrated-waveguide cavity," *International Journal of RF and Microwave Computer-Aided Engineering*, Vol. 30, No. 3, 2019.
18. Pasumarthi, S. R., J. B. Kamili, and M. P. Avala, "Design of tri-band MIMO antenna with improved isolation using DGS and Vias," *Wireless Personal Communications*, Vol. 110, No. 3, 2020.
19. Niu, B. and J. Tan, "Half-mode SIW cavity antenna for tri-band MIMO applications," *Microwave and Optical Technology Letters*, Vol. 62, No. 4, 1697–1701, 2020.
20. Rajeshkumar, V. and R. Rajkumar, "SRR loaded compact tri-band MIMO antenna for WLAN/WiMAX application," *Progress In Electromagnetics Research Letters*, Vol. 95, 43–53, 2021.
21. Adam, I., H. A. Rahim, et al., "Mutual coupling suppression in wearable MIMO antenna for on/off-body WBAN applications," *Journal of Physics: Conference Series*, Vol. 1755, 012011, 2021.
22. Hazarika, B., B. Basu, and A. Nandi, "Design of dual-band conformal AMC integrated antenna for SAR reduction in WBAN," *Progress In Electromagnetics Research C*, Vol. 110, 91–102, 2021.
23. Banerjee, J., A. Karmakar, R. Ghatak, and D. R. Poddar, "Compact CPW-fed UWB MIMO antenna with a novel modified Minkowski fractal Defected Ground Structure (DGS) for high isolation and triple band-notch characteristic," *Journal of Electromagnetic Waves and Applications*, Vol. 31, No. 15, 1–16, 2017.
24. Muhammad, I., N. Nguyen-Trong, and A. Abbosh, "Realization of a tapered slot array as both decoupling and radiating structure for 4G/5G wireless devices," *IEEE Access*, Vol. 7, 159112–159118, 2019.
25. Du, C., X. Li, and S. Zhong, "Compact liquid crystal polymer based tri-band flexible antenna for WLAN/WiMAX/5G applications," *IEEE Access*, 1–1, 2019.